XI ECCOMAS Thematic Conference on Smart Structures and Materials
SMART 2025
M. Krommer, M. Nader, M. Schagerl and A. Benjeddou (Eds)

AN INVESTIGATION OF STRUCTURAL STRESS IN ACTIVE ACOUSTIC BLACK HOLES

JORDAN CHEER*, AND ARCHIE KEYS*

*Institute of Sound and Vibration Research, University of Southampton
Highfield Campus, SO17 1BJ, Southampton, UK
e-mail: j.cheer@soton.ac.uk, web page: https://www.southampton.ac.uk/isvr

Abstract. Acoustic Black Holes (ABHs) are structural features that enable a notable level of vibration control by introducing a spatial variation in either the thickness or material properites of a structure, leading to a significant reduction in the wave speed and resultingly an increase in the efficiency of an applied damping treatment. There are two key potential limitations associated with ABHs – firstly, due to the focusing of structural waves into the ABH feature they can increase the structural stresses; and secondly, their performance at low frequencies is limited by the size of the ABH feature. It has previously been shown that through the integration of active control it is possible to enhance the low-frequency performance of ABHs, however, the effect that this has on the resulting stress has not been previously explored. This paper presents an investigation into the change in structural stress due to the integration of active control into an ABH terminated beam. A feedforward wave-based controller is utilised, which aims to minimise the wave reflected from the ABH termination using a piezoelectric patch actuator attached to the ABH feature. This demonstrates that a conventional active ABH introduces a significant stress enhancement and, therefore, a modified control strategy is explored in which the stress measured in the ABH is included in the cost function being minimised.

Key words: Active vibration control, Acoustic Black Holes, Structural Stress, Smart Structures

1 INTRODUCTION

High performing lightweight vibration control treatments are critical to a variety of industrial applications, including the automotive, aerospace, rail and maritime sectors. Since the observation of the Acoustic Black Hole (ABH) effect in structures with a decreasing thickness profile in the late 1980s [1], so-called ABHs have been extensively explored, as reviewed by Pelat et al [2]. ABHs are most commonly realised as structural features that are designed to control flexural waves and this is now classicaly realised by introducing a power-law decreasing thickness profile into a structure [1], as shown in

Figure 1 for a beam. This smooth impedance change results in a gradual decrease in the flexural wave speed and a corresponding decrease in its wavelength, which has now been widely shown to improve the efficacy of an applied damping layer [3, 4] and allow the ABH to offer an extremely high level of vibration control.

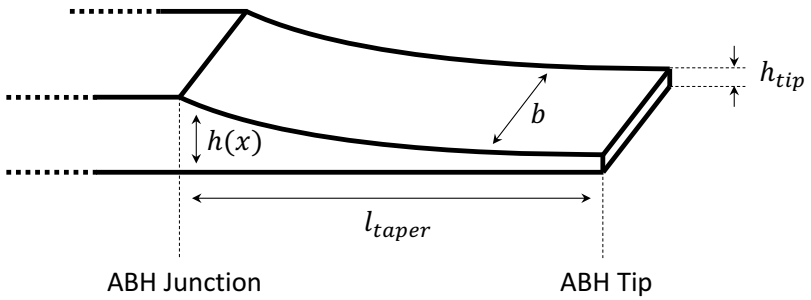

Figure 1: Diagram of a geometric ABH applied as a beam termination.

A wide variety of different ABH designs have been proposed, including extension to a two-dimensional design that can be embedded into plate-like structures [5], spiral ABHs that reduce the space required by the ABH taper [6], and multimaterial designs [7, 8]. In all of these cases the behaviour of the ABH can be tuned by modifiying the impedance, which in the geometrical ABH case can be controlled via the tip height, h_{tip}, taper length, l_{taper}, and taper profile, $h(x)$, as shown in Figure 1. Although these designs can be variously optimised [9] or tuned [10] to achieve broadband vibration control, the low frequency performance is essentially limited by the length of the ABH. It has been shown for both beam [11] and plate [12] applications that this low-frequency limitation can be overcome by incorporating active control into the ABH. In the beam case, the active ABH has been realised by applying a piezoelectric patch actuator to the ABH taper and driving this via either feedforward [12] or feedback [13] control stategies to control the reflected wave component. This has been shown to achieve very wideband control of the reflected wave and, interestingly, offer either a significant increase in performance or a significant reduction in the required electrical power compared to an equivalent active control system applied to a constant thickness beam.

Although geometric ABHs have been shown to offer significant levels of vibration control performance in both passive and active configurations, the thinness of the structure can pose issues in terms of the structural strength [15] and it has also been shown for passive ABHs that the wave focusing that is inherent to the ABH effect leads to stress concentration in the ABH taper due to high amplitude bending [14]. This can lead to a reduced useful life of the ABH structure and limit its application to practical engineering problems. This problem has been quite thoroughly explored for passive ABHs in beams [14], and modified ABH designs to reduce the stress have been proposed [16], however, an analysis of the stress in active ABHs has not been explored. This paper therefore ad-

dresses this gap by exploring through an experimental implementation of an active ABH terminating a beam, the influence of active control on the stress in the ABH taper. In the first instance, the previously proposed active ABH strategy is explored, which attempts to minimise the wave reflected from the active ABH beam termatinion, before an alternative control stategy is proposed in which the active ABH is driven instead to minimise the stress in the ABH taper. The paper is structured as follows: Section 2 describes the physical active ABH system realisation, Section 3 describes the two control strategies being considered, Section 4 presents the performance of the active ABH configurations in terms of the reflected wave and the stress in the ABH taper and Section 5 draws conclusions.

2 ACTIVE ABH SYSTEM DESCRIPTION

To investigate the behaviour of an active ABH system, the setup shown in Figures 2 and 3 has been implemented. The geometrical parameters defining the beam section and ABH taper are defined in Table 1. The ABH terminated beam was attached directly to a shaker, which provides the primary disturbance, and the control force is applied by a piezoelectric patch actuator attached to the flat side of the ABH termination to avoid applying a pre-stress to the actuator. A PI ceramic P-876.A11 actuator has been used, which has dimensions of 61 mm×31 mm and it has been positioned centrally across the width of the ABH and aligned with the tip to maximise the available bending force. The stress in the ABH taper has been measured using a strain gauge, which is applied to the curved side of the ABH taper and centred with resepct to both the length and the width of the taper. A Techni Measure PFL-30-11 strain gauge has been utilised, which has active dimensions of 30 mm×2.3 mm. This strain gauage has been selected so that the active area covers the main stress concentration region in the ABH due to bending, which has been identified via numerical simulations not reported here. The response of the beam has been measured using a pair of accelerometers, which are separated by a distance of $\Delta_x = 2$ cm, with their centre point being located 21 cm from the primary disturbance. All system responses have been measured at a sample rate of 24 kHz, with antialiasing and reconstruction filters set to 10 kHz.

Parameter	Symbol	Value
Beam thickness	h_0	10 mm
Beam length	l_{beam}	300 mm
Beam width	b	40 mm
ABH taper length	l_{ABH}	70 mm
ABH power law	μ	4
ABH tip height	h_{tip}	0.6 mm

Table 1: The geometrical parameters defining the geometry of the geometrical ABH shown in Figure 1.

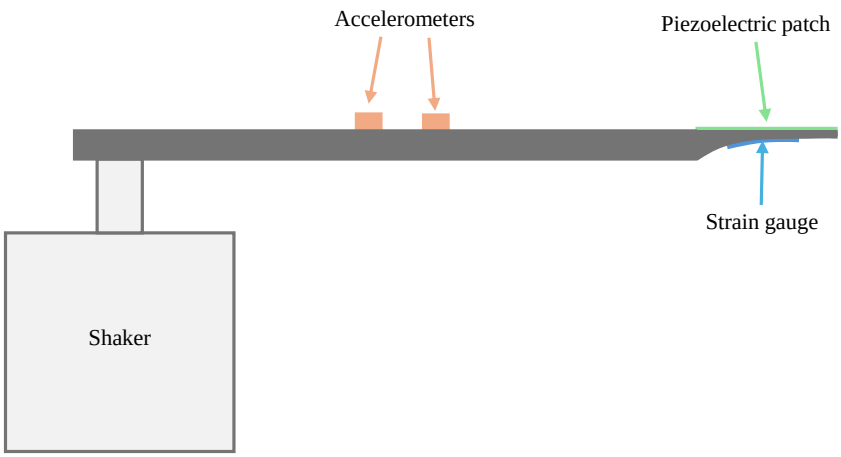

Figure 2: Diagram showing the experimental setup including two accelerometers mounted on the beam section, a piezoelectric patch actuator mounted on the flat side of the ABH termination and a strain gauage mounted on the tapered side of the ABH termination. The primary excitation is provided by a separate shaker to which the beam is mounted.

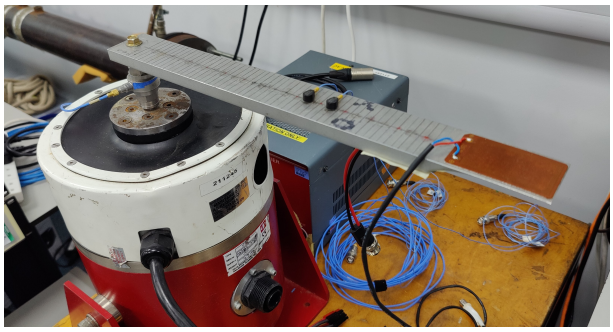

Figure 3: Photograph of the physical realisation of the system described in Figure 2.

3 CONTROL STRATEGIES

Active vibration control has been applied to a wide variety of structures using an even larger variety of control strategies. In the context of an ABH terminating a beam, the overall objective is generally to minimse the reflection from the end of the beam in order to realise an anechoic termination and thus supress the excitation of beam modes. An active anechoic termination applied to a uniform thickness beam has previously been developed in [17] and this strategy has been applied to an active ABH in [11]. This control strategy is first summarised in the following section, before an alternative control strategy is proposed which instead aims to reduce the stress in the ABH taper.

3.1 Reflection Control Strategy

The control strategy used to minimise the reflection from the end of the beam has been previously described in [11] and is outlined by the block diagram presented in Figure 4. From this block diagram it can be seen that this is a feedforward control strategy, where it is assumed for simplicity that the reference signal, $x(n)$, is provided directly from the primary excitation and the broadband controller, $\mathbf{w}$, is either adapted or optimised to minimise the reflected wave component, $e_{\phi^-}(n)$. It would be possible, and required in some practical installations, to instead utilise the incident wave component, $e_{\phi^+}(n)$, as the reference signal, although this complicates the controller design somewhat.

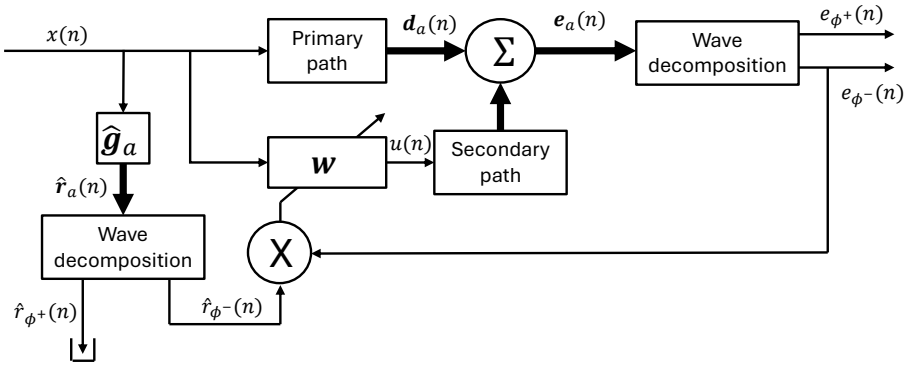

Figure 4: Block diagram showing the wave-based reflection control strategy [11].

In order to realise the feedforward control system shown in Figure 4, it is first necessary to decompose the vibration of the structure into the incident and reflected wave components. This can be achieved using the wave decompoisiton strategy outlined in [17, 11] which uses a pair of closely spaced accelerometers. This assumes that the accelerometer array is sufficiently far from any structural excitations or impedance changes, such as the tapering thickness profile in the ABH terminated beam, such that any evanescent wave

components will be small in magnitude compared to the travelling wave terms so that they can be neglected; the implications and limitations of this assumption are discussed in more detail in [11]. Following this approach, the incident and reflected wave components can be expressed in the frequency domain as

$$\begin{bmatrix} \phi^+(\omega) \\ \phi^-(\omega) \end{bmatrix} = \begin{bmatrix} H_1(\omega) & H_2(\omega) \\ H_2(\omega) & H_1(\omega) \end{bmatrix} \begin{bmatrix} A_1(\omega) \\ A_2(\omega) \end{bmatrix}, \tag{1}$$

where ω is the angular frequency, $A_1(\omega)$ and $A_2(\omega)$ are the complex amplitudes of the acceleration measured by the two accelerometers attached to the uniform beam section, and $H_1(\omega)$ and $H_2(\omega)$ are given by

$$H_1(\omega) = -\frac{1}{4\omega}\left(\frac{1}{\sin k_f \Delta_x/2} + \frac{i}{\cos k_f \Delta_x/2}\right) \tag{2}$$

$$H_2(\omega) = \frac{1}{4\omega}\left(\frac{1}{\sin k_f \Delta_x/2} - \frac{i}{\cos k_f \Delta_x/2}\right), \tag{3}$$

where k_f is the flexural wavenumber of the uniform beam section of the structure. In order to realise a broadband control solution, it is necessary to approximate the frequency domain wave decomposition operators, $H_1(\omega)$ and $H_2(\omega)$, using broadband filters, which can be achieved by inverse Fourier transformation and application of a modelling delay [18] to provide Finite Impulse Response (FIR) filters, $\mathbf{h}_1$ and $\mathbf{h}_2$. The incident and reflected wave components can then be expressed in the time domain as

$$\begin{bmatrix} \phi^+(n) \\ \phi^-(n) \end{bmatrix} = \begin{bmatrix} \mathbf{h}_1 & \mathbf{h}_2 \\ \mathbf{h}_2 & \mathbf{h}_1 \end{bmatrix} * \begin{bmatrix} a_1(n) \\ a_2(n) \end{bmatrix}, \tag{4}$$

where $a_1(n)$ and $a_2(n)$ are the outputs of each of the accelerometers at the nth time step.

The aim of the wave-based reflection controller is to minimise the cost function given as

$$J_{\phi^-} = \mathbf{E}\left[e^2_{\phi^-}(n)\right] + \beta \mathbf{w}^T \mathbf{w}, \tag{5}$$

where the first term relates to the magnitude squared reflected wave amplitude and the second term is proportional to the control effort, with the regularisation parameter β determining the weighting of the second term in the cost function. The error signal used in this cost function is given as

$$e_{\phi^-}(n) = \mathbf{h}_2^T \mathbf{e}_1(n) + \mathbf{h}_1^T \mathbf{e}_2(n), \tag{6}$$

where $\mathbf{h}_1$ and $\mathbf{h}_2$ are the wave decomposition FIR filters, each with I_h coefficients and $\mathbf{e}_1(n)$ and $\mathbf{e}_2(n)$ are the vectors comprising of the current and past samples of the error signals measured at the two accelerometers. This cost function can either be minimised

adaptively using the widely employed Filtered-reference Least Mean Squares (FxLMS) algorithm, or the optimal vector of control filter coefficients can be calculated directly as described in detail in [11]. The optimal control filter that minimises the cost function given by equation 5 is given as

$$\mathbf{w}_{\phi^-}^{(opt)} = -\left\{\mathbf{E}\left[\mathbf{r}_{\phi^-}(n)\mathbf{r}_{\phi^-}^T(n)\right] + \beta\mathbf{I}\right\}^{-1}\mathbf{E}\left[\mathbf{r}_{\phi^-}(n)d_{\phi^-}(n)\right], \tag{7}$$

where $\mathbf{E}$ is the expectation operator, $d_{\phi^-}(n)$ is the disturbance signal corresponding to the negative travelling wave and $\mathbf{r}_{\phi^-}(n)$ is the is the vector of current and past samples of the reference signal filtered by the secondary path, or plant response, between the control actuator and the negative propagating wave error signal.

3.2 Stress Control Strategy

As noted in Section 1, ABHs tend to exhibit high levels of stress concentration due to the wave focusing effect and the inherently thin structure when realised using geometrical tapering [14]. Although passive approaches to reducing the stress in ABHs have been explored [16], the interest here is to evaluate whether an active ABH can be utilised to reduce the stress in the ABH taper. To this end, instead of driving the control actuator to minimise the reflected wave, a new cost function can be defined as

$$J_\sigma = \mathbf{E}\left[e_\sigma^2(n)\right] + \beta\mathbf{w}^T\mathbf{w}, \tag{8}$$

where $e_\sigma(n)$ is the error signal measured by the strain gauge applied to the ABH taper as shown in Figure 2. In this case, the control block diagram is shown in Figure 5 which can again utilise the FxLMS algorithm, or the optimal vector of filter coefficients that minimises the cost function defined by equation 8 can be written as

$$\mathbf{w}_{\sigma}^{(opt)} = -\left\{\mathbf{E}\left[\mathbf{r}_{\sigma}(n)\mathbf{r}_{\sigma}^T(n)\right] + \beta\mathbf{I}\right\}^{-1}\mathbf{E}\left[\mathbf{r}_{\sigma}(n)d(n)_{\sigma}\right], \tag{9}$$

where $d_\sigma(n)$ is the disturbance signal measured by the strain gauge and $\mathbf{r}_\sigma(n)$ is the is the vector of current and past samples of the reference signal filtered by the secondary path, or plant response, between the control actuator and the strain gauge.

4 ACTIVE ABH CONTROL PERFORMANCE

To evaluate the performance of the two active control strategies described in Section 3, the measured primary and secondary path responses of the active ABH system shown in Figure 3 have been used to calculate the optimal control filters according to equations 7 and 9 for the reflection and stress control strategies respectively. The two control strategies are then evaluated via offline simulations using the measured responses. The reflection coefficient is calculated as

$$R(\omega) = \left|\frac{\phi_-(\omega)}{\phi_+(\omega)}\right| \tag{10}$$

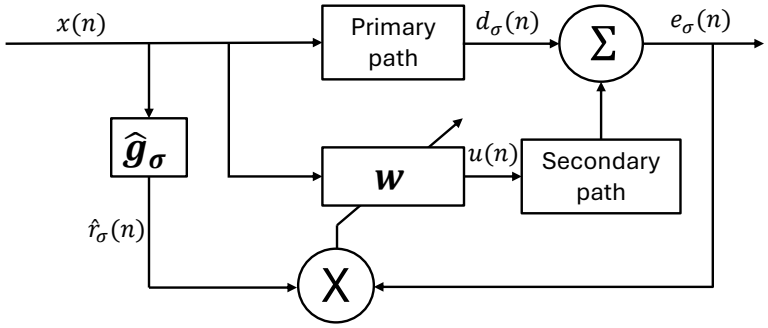

Figure 5: Block diagram showing the stress control strategy.

where $\phi_+(\omega)$ and $\phi_-(\omega)$ are the positive and negative travelling waves respectively, which can be calculated using the wave decomposition described in Section 3.1 for the uncontrolled case using the disturbance signals, d_1 and d_2, or the error signals, e_1 and e_2, for the corresponding controller. The stress in the taper is measured using the attached strain gauage, as shown in Figures 2 and 3, with the stress under control being calculated assuming linear superposition in the frequency domain as

$$e_\sigma(\omega) = d_\sigma(\omega) + g_\sigma(\omega)u(\omega), \tag{11}$$

where $g_\sigma(\omega)$ is the secondary path response between the piezo actuator and the strain gauage and $u(\omega)$ is the control signal generated by passing the reference signal through the corresponding optimal control filter for each control straetgy.

Figure 6 shows the reflection coefficient over frequency for the ABH terminated beam without control (black line) and with both the optimal reflection controller (red line) and the optimal stress controller (blue line). It is first worthwhile noting the characteristic reflection coefficient response of the passive ABH beam termination, which shows a general decrease in reflection with increasing frequency, but also exhibits dips in the reflection coefficient over frequency that correspond to modes of the ABH [10]. It is also worth highlighting that the passive ABH performance is already quite significant compared to an uniform thickness beam with an equivalent damping layer applied, which would have a reflection coefficient close to unity across the presented bandwidth, as previously shown in [11] for example. In the case of the reflection controller, as previous reported in [11], a significant decrease in the reflection coefficient across the presented bandwith is shown, corresponding to an effective increase in the absorption provided by the beam termination. There is some difficulty in achieving control at very low frequencies, which can be related to the low frequency limit of the piezoelectric actuator utilised, and would need to be addressed by selection of an alternative actuator or actuation approach. In the case of the stress controller, it can be seen that the reflection coefficient remains largely unchanged compared to the passive case.

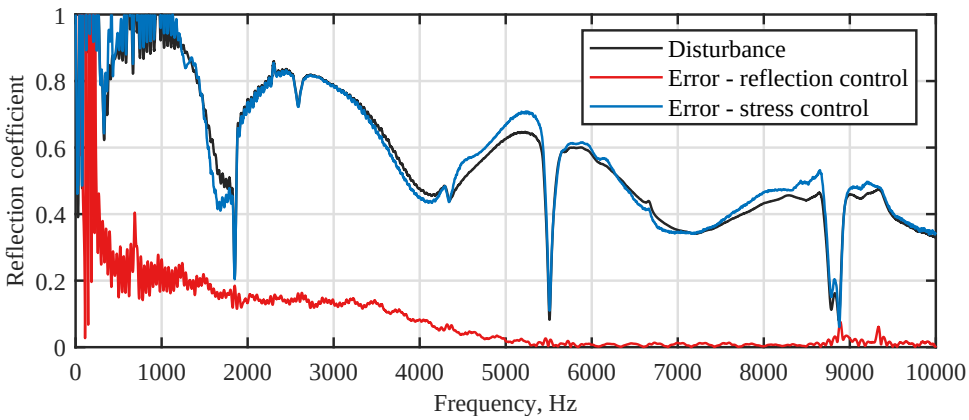

Figure 6: Reflection coefficient plotted over frequency for the ABH terminated beam without control (black line), with reflection control (red line) and with stress control (blue line).

Figure 7 shows the stress measured in the ABH taper without control (black) and with both the optimal reflection controller (red line) and the optimal stress controller (blue line). In this case it can be seen that the reflection control straetgy results in a significant increase in the stress across the whole of the presented bandwidth, except at a narrowband notch at around 8.8 kHz, which can be related to the high reflection control performance already achieved by the passive ABH at this frequency as shown in Figure 6. This is an important result as it demonstrates for the first time the trade-off that is paid for achieving high levels of reflection control using the active ABH termination and motivates the exploration of the active stress control strategy proposed here. The results presented in Figure 7 for the stress controller show a significant reduction in the stress in the ABH taper across the full frequency range presented compared to both the passive ABH and the active ABH using reflection control. This result suggests that the stress control approach could significantly extend the structural life of the ABH taper, although this is at the expense of the augmented reflection control provided by the active ABH termination using reflection control. It is also worth observing that this level of reduction in the ABH stress is significantly greater than that achieved via passive measures, as previously described in [16], but requires the addition of the piezoelectric actuator, strain gauage and controller. It is also interesting to note that the results presented here are consistent with previous work that explored the trade-off between controlling the reflected wave and the acceleration in the ABH taper using a weighted feedback control strategy [13]. However, in that case the stress was not directly observed and the controller required both the taper vibration and the reflected wave to be available whereas the strategy proposed here is potentially able to operate with a local control loop between the piezoelectric actuator and the strain gauage.

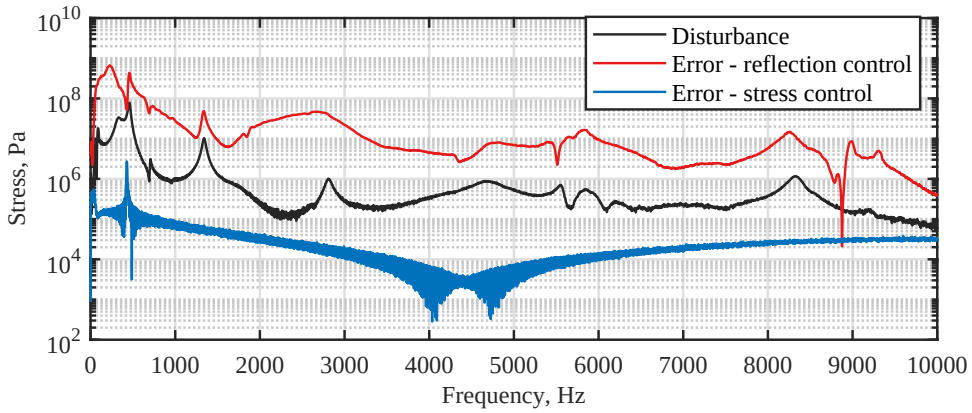

Figure 7: Stress plotted over frequency for the ABH terminated beam without control (black line), with reflection control (red line) and with stress control (blue line).

5 CONCLUSIONS

This paper has presented an investigation into the effect of actively controlling a geometric ABH terminating a beam on the stress in the ABH taper. An experimental implementation of an active ABH has been realised and the measured responses utilised to simulate the performance of two active control straetgies. In the first instance, the reflection control strategy that has previously been applied to ABHs has been explored and it has been shown that although significant levels of reflected wave control are achieved, this approach significantly enhances the stress in the ABH taper. To potentially overcome this increase in stress, an alternative control strategy is proposed that directly minimises the stress measured using a strain gauage attached to the ABH taper. In this case, a significant broadband reduction in stress is achieved, potentially providing a large increase in the structural life of the ABH taper, but the reflection coefficient performance in this case is equivalent to the passive ABH. This work demonstrates a clear trade-off between controlling the absorption provided by an active ABH beam termination and the resulting stress in the ABH taper. The two strategies offer the potential for designers to achieve one of these objectives depending on the requirements of the intended application. Due to the consistent architectures of the two control straetgies, depending on the importance of vibration control or structural life, it would be possible for control to switch between the two strategies. Future work will explore whether a trade-off between reflection control and stress control can be achieved by utilising a modified cost function and in the case of the stress control strategy a local feedback control approach may also be a convenient design approach.

ACKNOWLEDGEMENTS

This work was partially supported by the Intelligent Structures for Low Noise Environments (ISLNE) EPSRC Prosperity Partnership (EP/S03661X/1) and partially by the

Department of Science, Innovation and Technology (DSIT) and the Royal Academy of Engineering under the Research Chairs and Senior Research Fellowships programme.

REFERENCES

[1] Mironov MA (1988) Propagation of a flexural wave in a plate whose thickness decreases smoothly to zero in a finite interval. Sov. Phys. Acoust, 34(3), 318-319.

[2] Pelat A, Gautier F, Conlon F C and Semperlotti F (2020) The acoustic black hole: A review of theory and applications. Journal of Sound and Vibration. 476, 115316.

[3] Krylov VV (2004) New type of vibration dampers utilising the effect of acoustic 'black holes'. Acta Acustica united with Acustica, 90(5), 830-837.

[4] Krylov VV, and Tilman FJBS (2004) Acoustic 'black holes' for flexural waves as effective vibration dampers. Journal of sound and vibration, 274(3-5), 605-619.

[5] Krylov, V. V. (2007). Propagation of plate bending waves in the vicinity of one-and two-dimensional acoustic 'black holes'. ECCOMAS Thematic Conference on Computational Methods Rethymno, Crete, Greece.

[6] Lee, J. Y., and Jeon, W. (2017). Vibration damping using a spiral acoustic black hole. The Journal of the Acoustical Society of America, 141(3), 1437-1445.

[7] Austin, B., Cheer, J., and Bastola, A. (2022, August). Design of a multi-material acoustic black hole. In Proceedings of 2022 International Congress on Noise Control Engineering, INTER-NOISE2022.

[8] Austin, B., Cheer, J., and Bastola, A. (2023, December). Experimental validation of a multi-material acoustic black hole. In Proceedings of Meetings on Acoustics (Vol. 52, No. 1). AIP Publishing.

[9] McCormick C A and Shepherd M R 2020 Design optimization and performance comparison of three styles of one-dimensional acoustic black hole vibration absorbers J. Sound Vib. 470 115164

[10] Hook K, Cheer J, and Daley S (2019). A parametric study of an acoustic black hole on a beam. The Journal of the Acoustical Society of America, 145(6), 3488-3498.

[11] Cheer J, Hook K, and Daley S. (2021) Active feedforward control of flexural waves in an Acoustic Black Hole terminated beam. Smart Materials and Structures, 30(3), 035003.

[12] Hook K, Cheer J, and Daley S. (2022). Control of vibration in a plate using active acoustic black holes. Smart Materials and Structures, 31(3), 035033.

[13] Hook K, Daley S., and Cheer J (2022). Active control of an acoustic black hole using a feedback strategy.Journal of Sound and Vibration, 528, 116895.

[14] Keys A, and Cheer J (2024, October). A parametric study of dynamic stress in acoustic black holes. In INTER-NOISE and NOISE-CON Congress and Conference Proceedings (Vol. 270, No. 3, pp. 8410-8421). Institute of Noise Control Engineering.

[15] Zhou, T., Tang, L., Ji, H., Qiu, J., and Cheng, L. (2017). Dynamic and static properties of double-layered compound acoustic black hole structures. International Journal of Applied Mechanics, 9(05), 1750074.

[16] Keys A, and Cheer J. (2024, September). Optimisation of a modified acoustic black hole profilefor the reduction of dynamic stress. In ISMA2024 Proceedings.

[17] Rustighi, E., Mace, B. R., and Ferguson, N. S. (2011). An adaptive anechoic termination for active vibration control. Journal of Vibration and Control, 17(13), 2066-2078.

[18] Mace, B. R., and Halkyard, C. R. (2000). Time domain estimation of response and intensity in beams using wave decomposition and reconstruction. Journal of Sound and Vibration, 230(3), 561-589.